First-principles Study of Magnetism and Electronic Structure of Li_xFePO_4

D. Odkhuu[1*], T. Tsevelmaa[1], N. Tsogbadrakh[2] and S. C. Hong[1]**

[1] *Department of Physics and Energy Harvest-Storage Research Center, University of Ulsan, Ulsan 680-749, Republic of Korea*
[2]*Department of Theoretical Physics, School of Physics and Electronics,*
National University of Mongolia, University Strteet-1, Ulaanbaatar-210646, Mongolia
**E- mail: odkhuu_d@yahoo.com*
***E- mail: tsogbadrakh@num.edu.mn*

$LiFePO_4$ have attracted a great interest as a cathode material for Li rechargeable batteries. In this study we evaluated the magnetism emphasizing on magnetization axes and electronic structures of the olivine phases of Li_xFePO_4 ($0 \le x \le 1$) by means of density-functional theory. We show that the insertion/extraction of lithium affects slightly the magnetic moment of Fe, but the spin orientations in antiferromagnetic ground state are found to be noteworthy. The easy magnetization axis of $FePO_4$ is along [010], whereas it is on [001] for $LiFePO_4$, in consistent with an experiment. The use of exchange-correlation U parameter in the electronic structure calculations describes well the observed insulating characters of $FePO_4$ and $LiFePO_4$.

Keywords: Li_xFePO4, First-principles, Magnetism, Magnetocrystalline anisotropy, Band structure, Density of states

PACS number(s): 82.47.Aa, 75.10.Dg, 75.30.Gw, 75.50.Ee

I. INTRODUCTION

The rechargeable Li-ion battery is one of the most attractive and useful technology among rechargeable batteries due to the highest energy density preserving low weight and small volume. An electric vehicle, hybrid electric vehicle, and stationary energy storage are certainly modern and future applications of the rechargeable Li-ion battery beyond its current commerce in portable electronic devices.

In recent years, lithium phosphate compounds ($LiMPO_4$, M is a transition metal) have been extensively and intensively studied as promising cathode materials for Li-ion rechargeable batteries [1-7]. Among them, in particularly, the iron-based $LiFePO_4$ is mostly attracted because the iron is low cost natural abundance, environmentally friendliness, i.e. less toxic and safe in operation than other transition metals such as Co, Ni, and Mn. Even though its appreciable properties of a high theoretical capacity (170 mAh/g) [2], a high intercalation voltage (3.5 V) [3], long cycle life (up to 2000), good structural stability during charging/discharging, $LiFePO_4$ exhibits a low electronic and ionic conductivity in order of 10^{-8}-10^{-9} Scm^{-1} [8,9,10]. This low conductivity problem has been devoted by some attempts such as a carbon coating [11,12], cation doping [13,14], and controlling particle size [6,15]. However, each of them to improve electronic conductivity or electrochemical performance has not been perfected as is expected. This has led to future extensive challenges to clarify one's inherent features. Indeed the intrinsic magnetic properties including magnetization easy axis should be supplied in order to understand its basic physical phenomena because the electronic state is, in principle, reflected by a magnetic property, which govern the charge storage and electronic conductivity, as well as electrochemical reaction mechanism. In other words, the magnetism in such materials used in a battery technology might play a role at least in terms of microscopic origin of electronic structure.

$LiMPO_4$ has an antiferromagnetic (AFM) ground state. There have recently been interesting experimental studies on magnetization orientations [16-22]. The magnetic structures of $LiMPO_4$ (M=Mn, Ni, Co, and Fe) compounds crystallized in same olivine structure are determined to be collinear AFM state but with different spin directions. For example, in $LiCoPO_4$ the magnetic moments are oriented along the [010] direction [18] while they point along the [001] in $LiNiPO_4$ [21,22]. More interestingly, different magnetization direction on Fe atoms have been observed to be collinear AFM spin along the [010] for $LiFePO_4$ whereas it is turned almost along the [001] in $FePO_4$ by a neutron diffraction by G. Rousse *et al.*[17]. Further the AFM transitions of $FePO_4$ and $LiFePO_4$ occur at the Neel temperatures of 125 K and 50 K, respectively. Surprisingly, very few theoretical works have been considered the applicability of magnetic properties in magnetic Li-ion transition materials [23,24,25]. Very recently, Yamauchi and Picozzi performed the firs-principles calculation to demonstrate the magnetic

anisotropy and magnetoelectricity of $LiCoPO_4$ and $LiNiPO_4$ [25].

In this study, we examine the influence of lithium extraction/insertion, expressed as Li_xFePO_4 (x=0, 0.25, 0.5, 0.75, 1), where x is the concentration of Li ions that are extracted/inserted from/to the unit cell, on the magnetism and electronic structure from a first-principles density-functional theory. A fact that is verified that the magnetization direction can be switched with Li atoms in consistent with observations [17], where the e_g state near the Fermi level is responsible in terms of the density of states (DOS). We finally suggest that the excitation of magnetic properties, i.e. reorientation of magnetization, with respect to Li concentration may be an important associating their electronic structures for the mechanism of the Li-ion batteries.

II. COMPUTATIONAL METHOD

The density-functional theory calculations using the pseudo-potential projector-augmented wave (PAW) method were performed as implemented with the Vienna *ab initio* simulation package (VASP) code [26,27]. The exchange-correlation energy of electrons is described as the generalized gradient approximation (GGA) of Perdew, Burke, and Ernzerh (PBE) [28]. To describe Coulomb interaction among Fe-3*d* electrons, we have also taken into account a Hubbard model in the GGA (GGA+U) [29], which is known to be appropriate treatment for the insulating or semiconducting characters in strongly correlated materials of oxide alloys with 3*d* metals [29,30,31]. We have performed the test calculations with different choices of the effective U parameter (U_{eff}) values, in range of 3.5-4.5 eV. Among them, the 4.3 eV is used as U_{eff} value for the calculations of Li_xFePO_4, which gives an appropriate solution of the band gap observed in experiments. The valence electrons are described as $2s^1$ for Li, $3d^74s^1$ for Fe, $3s^23p^3$ for P, $2s^22p^4$ for O atom in pseudo-potentials calculations. A cutoff energy of 500 eV was chosen for the plane wave expansion of the wave functions. The Monkhorst-Pack scheme [32] with 4×6×8 *k*-point mesh in the Gaussian method [33] which in present systems gives quite reasonable results for total energy and magnetic configurations was used for the Brillouin zone integration, that consistent with experiments. To optimize the systems, full relaxation for both the atomic positions and lattice parameters for each x was taken into account. At low temperature, both $FePO_4$ and $LiFePO_4$ have an orthorhombic olivine with a space group of Pnma [1,10,34], which is shown in Fig. 1. The unit cell contains four formula units with 24 atoms (four Fe and four P, and sixteen O atoms) for x=0 and 28 atoms for x=1.

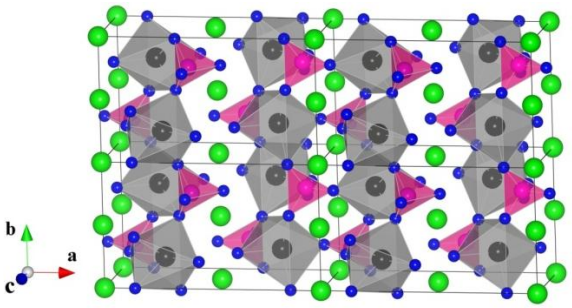

Figure 1. The 2×2×1 olivine structure of $LiFePO_4$. Big green and small blue balls are Li and O atoms, respectively. Fe atoms have octahedral environment with O atoms, while P do the tetrahedral

Phosphor has a tetrahedral site at the center of a 4-Oxygen cluster (PO_4) and iron occupies an octahedral site at the center of a cluster of six oxygen atoms (FeO_6) within the crystal. The coexistence of two phases of $FePO_4$ and $LiFePO_4$, biphase alloy as formulated $xLiFePO_4+(1-x)FePO_4$, is observed during charging and discharging ($0 < x < 1$) at room temperature. However, the mixed valence solid solution was recently observed at high temperature above 200 ^oC, at the same time the structural stability is well kept through the migration of Li^+ ions and corresponding electrons between $FePO_4$ and $LiFePO_4$ [35,36]. Thus we used a single crystal structure with same unit cell of $FePO_4/LiFePO_4$ for x=0.25, 0.5, and 0.75.

III. RESULTS AND DISCUSSION

In order to optimize the systems, we did systematically a serious of calculations as follows: *First*, the four (three) different atomic structures with Li ion and Li vacancy for x=0.25 and 0.75 (x=0.5) have been calculated. Namely, Cor-, Cen-, (100)-, (010)-type structure if a Li ion places respectively at the corner site (0.0, 0.0, 0.0), at the center site (0.5, 0.5, 0.5), on the (100) plane (0.0, 0.5, 0.0), on the (010) plane (0.5, 0.0, 0.5) in x=0.25, whereas a Li vacancy in the case of x=0.75. For x=0.5, the same notation of x=0.25 is used with the fixed one Li ion at the corner. For clarifying, atomic structures of Li_xFePO_4 for (a) x=0, (b) x=0.25, (c) x=0.5, (d) x=0.75, and (e) x=1 are

shown in Fig. 2, where the (010)-type atomic configurations are depicted exception of the Cen-type structure of $Li_{0.75}FePO_4$. *Second*, according to possibility of the magnetic configurations in a magnetic system, for each of above atomic structure including $FePO_4$ and $LiFePO_4$ we have performed the calculations with both ferromagnetic (FM) and three AFM configurations of Fe atoms: (i) Fe1(↑)Fe2(↑)Fe3(↓)Fe4(↓) (denoted as AFM-1), (ii) Fe1(↑)Fe2(↓)Fe3(↑)Fe4(↓) (AFM-2), and (iii) Fe1(↑)Fe2(↓)Fe3(↓)Fe4(↑) (AFM-3). The total energies for x=0, 0.25, 0.5, 0.75, and 1 of Li_xFePO_4 with all the possible atomic and magnetic structures are summarized in Table 1. For each value of x, the lowest energy is chosen as zero. The total energy differences, E_{tot}(AFM)-E_{tot}(FM), between FM and AFM are also shown in Table 1 and the calculated results for all x are negative. This clearly shows that Li_xFePO_4 is low temperature AFM. The decrease of ΔE with x indicates that experimentally the Neel temperatures of 125 and 50 K are well confirmed by our theoretical trends. Calculations show that the stability of magnetic structures is rather sensitive, but not strongly on the atomic configurations for x=0.25 and 0.75. In contrast, it is a quite fluctuating from both configurations in $Li_{0.5}FePO_4$. The AFM-1 phase is energetically the most favorable compared to other AFM configurations as well as FM regardless of Li concentration, in consistent with the experimental [16,17] and other theoretical works [23,24]. As before-mentioned, there are four environmentally different Li sites in the unit cell: one, two, and three Li atoms are for x=0.25, 0.5, and 0.75, respectively. When x=0.25 a Li atom may occupy one of the four sites, and as seen in Table I, the (010)-type structure of AFM-1 is more stable than the Cor-, Cen-, and (100)-type structure by 0.16, 0.25, and 0.03 meV/f.u., respectively. The most stable atomic structures from total energy calculation are shown as projected on 2D *ab*-plane in Fig. 2. Further insertion of Li atoms to the unit cell leads that first all possible Li atoms settle on the (010) face before the other sites are filled in the all x structures, implying that the diffusion of Li ions along the [010] calculated in previous theoretical studies [37,38].

Table 1. Total energies of different atomic and magnetic structures of Li_xFePO_4 for Li concentrations. Energy differences, $\Delta E=E_{tot}(AFM)-E_{tot}(FM)$, between FM and AFM for most stable configuration are also given. The unit of energy is in meV/f.u.

Li_xFePO_4	AFM-1				AFM-2				AFM-3				ΔE
	Cor	Cen	(100)	(010)	Cor	Cen	(100)	(010)	Cor	Cen	(100)	(010)	
x=0			0				85.67				49.01		-121.55
x=0.25	0.16	0.25	0.03	0	50.77	50.76	50.73	50.69	2.21	2.75	2.21	2.75	-76.18
x=0.5	-	7.17	89.94	0	-	58.04	119.57	47.70	-	14.65	96.02	3.81	-61.46
x=0.75	1.16	0	0.005	0.037	34.89	34.89	34.89	34.96	7.94	7.87	7.90	7.87	-44.39
x=1			0				17.24				6.20		-25.45

According to previous first-principles calculations of $FePO_4$ and $LiFePO_4$ [10], the DFT+U method usually gives qualitatively comparable results on particularly electronic structures with an experiment than GGA (LDA). Therefore, we also estimate the effect of U parameter on the GGA. With the most stable atomic and magnetic configurations, we present the optimized lattice parameters with cell volume within the GGA and GGA+U in Fig. 3. The experimental lattice parameters obtained from neutron diffraction measurement at 300 K are *a*=9.7599 Å, *b*=5.7519 Å, *c*= 4.7560 Å for $FePO_4$ and a=10.3377 Å, b=6.0112 Å, c=4.6950 Å for $LiFePO_4$ [17]. The lattice parameters (9.9113, 5.9189, 4.8725 Å) obtained from the GGA are slightly larger as compared to those (9.8642, 5.8836, 4.8531 Å) of GGA+U method for $FePO_4$, whereas it is smaller in case of $LiFePO_4$ (10.3944, 6.0475, 4.7315 Å for GGA and 10.4317, 6.0723, 4.7419 Å for GGA+U). At x=0.5, the lattice parameters for both exchange-correlation methods are almost identical. The agreement between the calculated results using the GGA and experimental ones for $LiFePO_4$ is greater as compared with the GGA+U, whereas the use of GGA+U leads better description for FePO4. Overall the calculated values of *a*, *b*, and *c* agree reasonably with the experimental (less than 1.5 % of deviations) and previous theoretical results. Thus we conclude that both the GGA and GGA+U allow for a good description to structural features. As seen in figure, two longer edges of *a* and *b* are extended with increasing x, whereas the shortest edge (*c*) is

compressed. As a result, the cell volume is found to increase by 2.5 % from $FePO_4$ to $LiFePO_4$. This small volumetric expansion and structural stability during Li ion insertion and extraction are suggested to be responsibility to a high cycle, as mentioned somewhere.

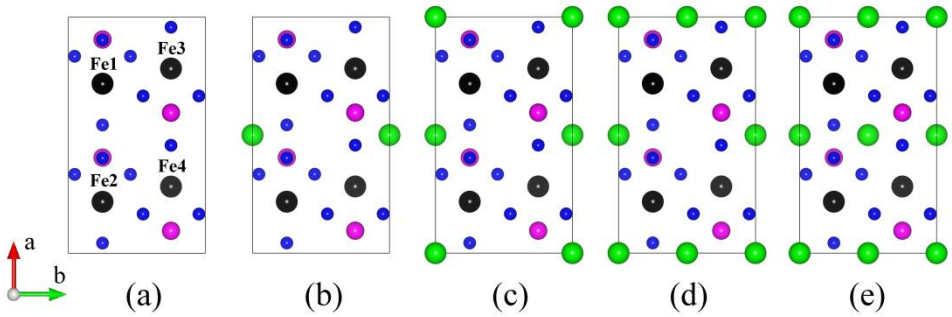

Figure 2. Top view of the optimized atomic structures of Li_xFePO_4 for (a) x=0, (b) x=0.25, (c) x=0.5, (d) x=0.75, (e) x=1. The optimized atomic positions of Fe sites are as follows, as an example of x=0: Fe1 (0.2745, 0.25, 0.9517), Fe2 (0.7747, 0.25, 0.5443), Fe3 (0.2253, 0.75, 0.4520), and Fe4 (0.7255, 0.75, 0.0446).

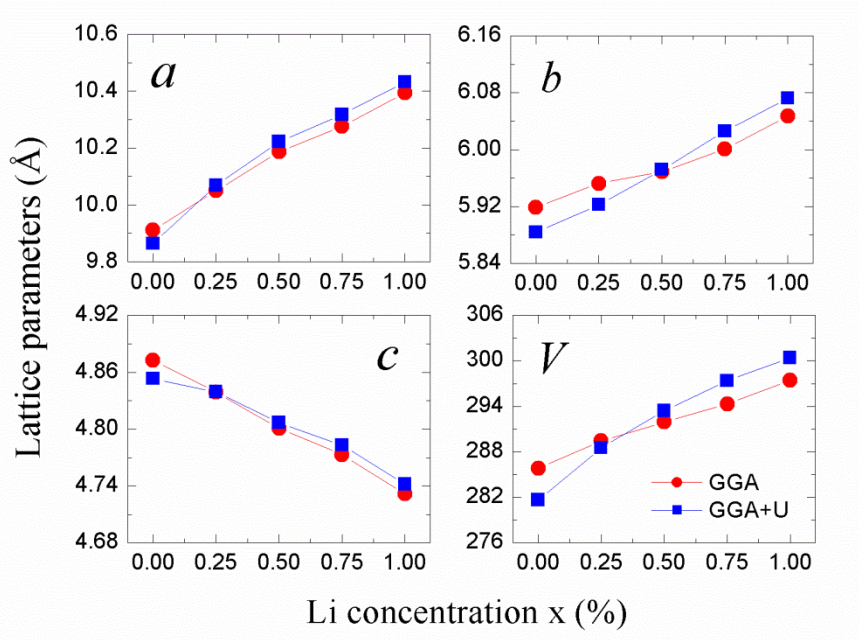

Figure 3. The optimized lattice parameters of a, b, and c (in Å), and cell volume V (in $Å^3$) of Li_xFePO_4 as functions of Li concentrations. Circle (square) symbols denote the calculated results from GGA (GGA+U) method.

To confirm the experimentally different crystallographic antiferromagnetism of $FePO_4$ against $LiFePO_4$ [16,17], we calculated the E_{MCA} between three different axes with collinear configurations since the total energy along *a*, *b*, and *c* axes are distinctive in an orthorhombic structure. Table 2 shows the calculated local magnetic moment of Fe atom and E_{MCA} between the [100] and [001], and [010] of Li_xFePO_4 within two different exchange-correlation approaches. Both the GGA and GGA+U result the Neel-type AFM configurations, i.e. zero net magnetization in the unit cell, but a Hubbard correction leads to more localized moments on Fe, increasing about 0.2-0.3 μ_B for each of x values. However, general trend of decreasing magnetic moment with increase of Li concentration is supplied by both methods, in consistent with observed moments of 4.96 μ_B for $FePO_4$ and 4.19 μ_B for $LiFePO_4$ [16,17]. The calculated spin magnetic moments are 3.96 (4.29) and 3.56 (3.77) μ_B for x=0 and 1 using the GGA (GGA+U), respectively. Typically the net moments are slightly underestimated in the computation, which is commonly observed in olivine structures due to the spin transfer of oxygen ions [23]. The calculated and measured magnetic moments are

also consistent with the crystal field theory for high spin states of the Fe^{2+} ($3d^6$) of $LiFePO_4$ and the Fe^{3+} ion ($3d^5$) of $FePO_4$. The crystal field energy is lower than the pairing energy and the ground states of six orbitals of Fe^{2+} are split to three spin up paired with one spin down electron at low energy t_{2g} orbital and the higher energy e_g orbital is filled by the rest of two electrons with spin up state, ($t_{2g}^{3\uparrow} e_g^{1\uparrow}, t_{2g}^{1\downarrow}$). For the Fe^{3+} ion, each of five t_{2g} and e_g orbitals is occupied with the unpaired spin up electron, ($t_{2g}^{3\uparrow} e_g^{1\uparrow}, t_{2g}^{0\downarrow}$). Therefore, according to Hund's rule, the net moments by the unpaired electron spin counts of Fe^{3+} and Fe^{2+} are 5 and 4 μ_B in high spin state.

The calculated E_{MCA}'s are found to be very anisotropic. The negative values of the calculated $E_{MCA}(E_{100}\text{-}E_{010})$ and ($E_{100}\text{-}E_{001}$) of $FePO_4$ indicate that the easy magnetization axes is along the [100]. Even though the magnetization direction of [100] is favored from [001] by energy difference of -0.86 meV/f.u. for $LiFePO_4$, the larger energy difference in positive sign between the [100] and [010] express that the [010] is the easy magnetization axis, in contrast to that in $FePO_4$.

Table 2. The magnetic moments (μ_B) of Fe sites and E_{MCA} (in meV/f.u.) between different crystallographic directions along the [100] and [100], [100] and [010]. The calculated results from the GGA and GGA+U are also given.

Li_xFePO_4	Fe1/Fe2		Fe3/Fe4		$E_{MCA}(E_{100}\text{-}E_{001})$		$E_{MCA}(E_{100}\text{-}E_{010})$	
	GGA	GGA+U	GGA	GGA+U	GGA	GGA+U	GGA	GGA+U
x=0	3.96	4.30	-3.96	-4.30	-0.06	-0.21	-0.18	-0.09
x=0.25	3.88	4.18	-3.88	-4.18	-0.45	-0.17	0.13	0.05
x=0.5	3.81	4.08	-3.81	4.08	-0.76	-0.15	0.46	0.94
x=0.75	3.70	3.92	-3.70	-3.92	-0.28	-0.09	0.99	0.36
x=1	3.56	3.77	-3.56	-3.77	-0.86	-0.02	1.14	0.25

Thus a rather good agreement between theory and experiment is obtained in our study. As x increases, the effect of Li ion (We have done a test calculation to clarify whether the insertion of Li ion affects to magnetization axes or it is a sensitive on a volume expansion. The calculated E_{MCA}s of $FePO_4$ used the lattice parameters of $LiFePO_4$ are -0.05 and -0.11 meV/f.u. for $E_{100}\text{-}E_{010}$ and $E_{100}\text{-}E_{001}$, respectively. The effect of volume expansion on magnetization axes is negligible.) turns out the spin direction on Fe site from [100] to [010]. There is no remarkable difference between the GGA and GGA+U on the magnetization axes, but quantitative divergences are observed, generally U decrease the E_{MCA}. This deficiency will clearly be observed in electronic structures calculation.

Our calculated band gaps are comparable to other theories, 0.1-0.5 eV for FePO4 and 0-0.53 eV for $LiFePO_4$ [10,23,24,39]. Nevertheless, the experimentally energy band gaps of 1.7 and 3.7-4.0 eV are observed for $FePO_4$ and $LiFePO_4$, respectively [5,6,10,40]. This deficiency of electronic structures was corrected by Zhou *et al.* using the GGA+U correction [10]. In this instruction, the band structures in the calculations of GGA+U have been also plotted for $FePO_4$ and $LiFePO_4$ in Fig. 5.

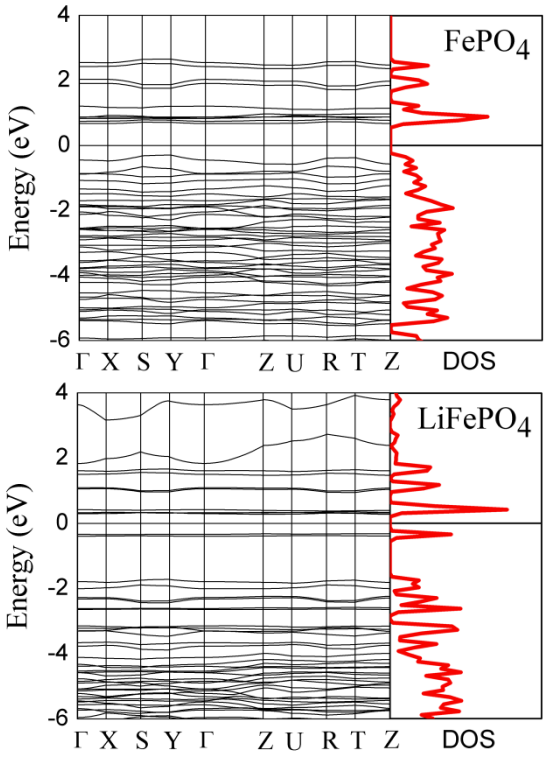

Figure 4. The electronic band structures and the density of states of $FePO_4$ (upper panel) and $LiFePO_4$ (lower panel) from the GGA calculation. The Fermi level is set to zero energy.

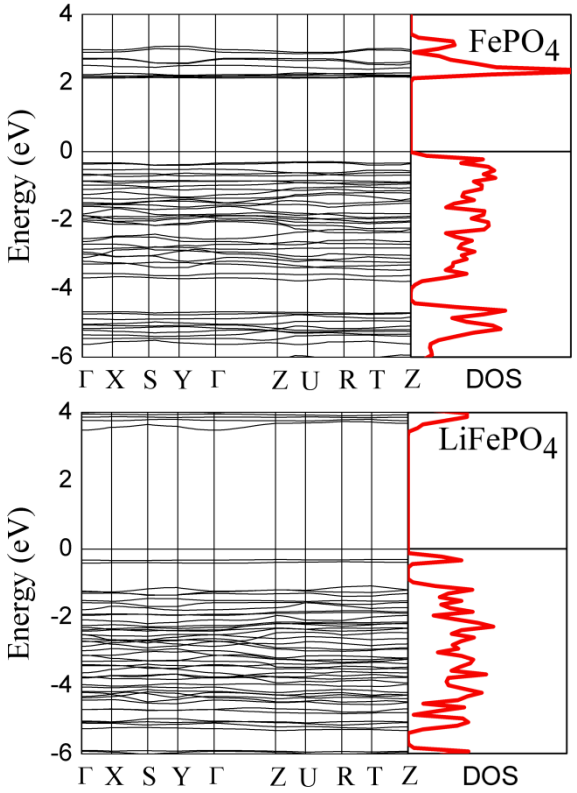

Figure 5. The band structures and the density of states of $FePO_4$ (upper panel) and $LiFePO_4$ (lower panel) from the GGA+U calculation. The energy level is set to zero energy.

Comparing with pure GGA, the electronic characteristic is very different and the conduction bands shift upward far from the Fermi level by about 1.4 eV for $FePO_4$, which results opening broad band gap of 2.05 eV. Correspondingly for $LiFePO_4$, a very tiny band gap of 0.42 eV in pure GGA, the use of GGA+U leads to significant enlargement to a more realistic value of 3.7 eV with U correction, in consistent with experiments. This is also in good agreement with electronic structure calculations used U as mentioned before. In conclusion to electronic structures, this study has shown that both GGA and GGA+U approaches are valid to describe the valence electronic structure, but the utilization of GGA is unable for the conduction bands, in resulting inappropriate solution for the band gap.

In order to elucidate the magnetic properties, we present the DOS of Fe atom for Li_xFePO_4 with x=0, 0.25, 0.5, 0.75, and 1 (from upper to lower panel) in Fig. 6. The left (right) panel in the figure shows the calculated DOS of Li_xFePO_4 from the GGA (GGA+U) method. The DOSs split to the spin-up and spin-down state, and the dotted (solid) lines represent t_{2g} (e_g) states.

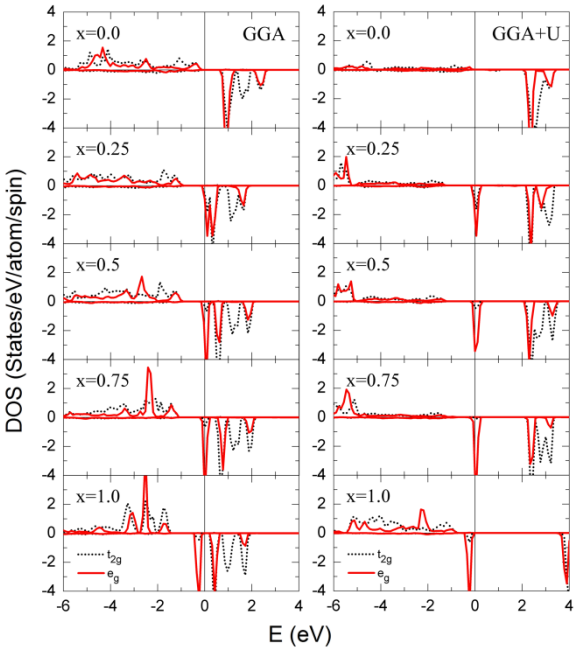

Figure 6. The local density of states of Fe atom in Li_xFePO_4 for x=0, 0.25, 0.5, 0.75, and 1. Left and right panel correspond to the GGA and GGA+U, respectively. The Fermi energy is set to zero energy.

With increase of x, the Fermi level shifts to the unoccupied state since the increase of the number of electrons in the unit cell. Eventually the Fermi level lies just above the new occupied valence band and below the bottom of the conduction band, creating a semiconductor band gap. The features of Fe DOS between the GGA and GGA+U are resemblance to the total DOS (Fig. 4 and 5); a localization of the valence electrons is rather than to the delocalized conduction electrons (upward shift) due to U effect. The DOS in the unoccupied band is wholly contributed by Fe 3*d* electrons for x=0 and 1, and also the occupied band near the Fermi level for x=1. The band gaps in Li_xFePO_4 are purely determined by Fe, indicating that for Fe site doping or substitution may alter an electronic state near the Fermi level [41,42]. The occupied spin-up Fe 3*d* states strongly hybridize with O 2*p* states, and lowest energy states are donated by the states of O atom. For $LiFePO_4$, the strong magnetic exchange-splitting between the spin-up and spin-down state of $FePO_4$ is reduced, i.e. decreasing magnetic moment as shown in Table II, due to the sharp e_g peak just below the Fermi level. The easy magnetization axis is altered from along *a*- to along *b*-axis when Li is inserted to $FePO_4$. At the same time, strong e_g and t_{2g} peaks shift to the occupied state and place near the Fermi level. But, the U correction pushes the t_{2g} state to higher energy

region and remains the e_g state at the Fermi level in Fig. 6. Due to the insensitivity of easy magnetization axes on the U parameter, the reorientation of magnetization direction is originated by the contribution of e_g state at/near the Fermi level. Furthermore, we demonstrate that partially intercalated single crystal structures are compensated half-metallic regardless of exchange-correlation approach for a given x, if the solid solution phase would be realized, in contrast to the insulating of $FePO_4$ and $LiFePO_4$. This might be a solution to improve the electronic conductivity. The charge density counter plots on the (0,1/4,0) plane for $FePO_4$ and $LiFePO_4$ are presented in Fig. 7(a) and 7(b), respectively. The charge distribution of Fe atoms is isotropic spherical in $FePO_4$, while it is anisotropic distribution toward to the e_g orbital for $LiFePO_4$. This suggests that the degenerated t_{2g} and e_g states of $FePO_4$ are strongly localized in the majority spin state and more pronounced e_g states of $LiFePO_4$ in the both spin channel in Fig. 6. The covalent bond between Fe and its nearest neighbor O atoms is considerably weakened, indicating that Fe loss its electrons with t_{2g} state during Li insertion. The distribution of O atoms tends to P atoms since their inter-atomic distance in tetrahedral environment is shorter than that of Fe-O with octahedron. As seen in Fig. 7(a) and (b), there is no significant difference of the distribution on P and O atoms between $FePO_4$ and $LiFePO_4$, implying that no charge transfer between P and O atoms is occurred during charging/discharging.

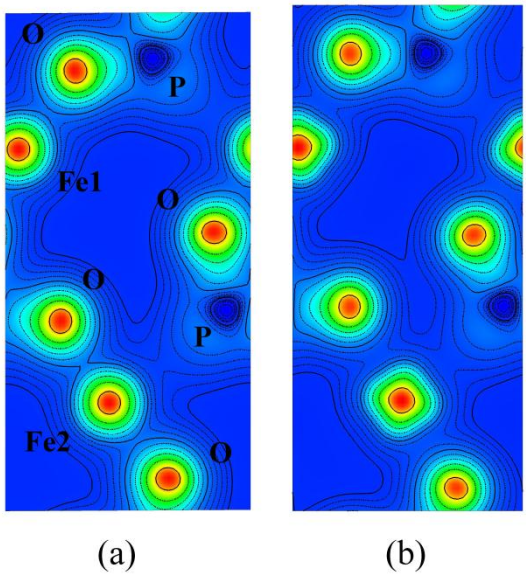

Figure 7. The charge densities of (a) $FePO_4$ and (b) $LiFePO_4$ on the (0,1/4,0) plane.

IV. CONCLUSION

First-principles density-functional theory has been employed to the effect of Li on magnetic and electronic properties of the olivine phase Li_xFePO_4. Total energy calculations show that an AFM state is more stable by the energy difference of about 0.12 (x=0) and 0.03 eV/f.u. (x=1) than a FM state, in consistent with experiments in which the AFM orderings of $FePO_4$ and $LiFePO_4$ were found at T_N=125 K and at T_N=50 K, respectively. The calculated magnetic moments of 3.56-3.96 μ_B for the GGA and 3.77-4.29 μ_B for the GGA+U are varied as functions of Li concentration. Consistent with observations, a different easy magnetization axes between x=0 (along *a*-axis) and x=1 (along *b*-axis) reflects also the differences between their electronic structures, where the e_g state is found to be a crucial. Both GGA and GGA+U approaches are valid to describe the valence electronic structure, but only the utilization of GGA+U is able for the conduction bands, in resulting appropriate solution for the band gaps. We also predict that partially intercalated single crystals (x=0.25, 0.5, and 0.75), which were synthesized at high temperature recently as solid solutions, are compensated half-metallic regardless of the exchange-correlation approaches.

REFERENCES

[1] A. K. Padhi, K. S. Nanjundaswamya, and J. B. Goodenough, J. Electrochem. Soc. **144**, 1188 (1997).
[2] H. Huang, S. C. Yin, and L. F. Nazar, Electrochem. Solid-State Lett. **4**, A170 (2001).
[3] M. S. Islam, D. J. Driscoll, C. A. J. Fisher, and P. R. Slater, Chem. Mater. **17**, 5085 (2005).
[4] M. Yonemura, A. Yamada, Y. Takei, N. Sonoyama, and R. Kanno, J. Electrochem. Soc. **151**, A1352 (2004).
[5] A. Yamada and S. C. Chung, J. Electrochem. Soc. **148**, A960 (2001).
[6] A. Yamada, S. C. Chung, and K. Hinokuma, J. Electrochem. Soc. **148**, A224 (2001).
[7] N. Bramnik, K. Bramnik, T. Buhrmester, C. Baehtz, H. Ehrenberg, and H. Fuess, J. Solid-State Electrochem. **8**, 558 (2004).
[8] C. Delacourt, L. Laffont, R. Bouchet, C. Wurm, J. B. Leriche, M. Morcrette, J. M. Tarascon, and C. Masquelier, J. Electrochem. Soc. **152,** A913 (2005).

[9] B. Ellis, L. K. Perry, D. H. Ryan, and L. F. Nazar, J. Am. Chem. Soc. **128**, 11416 (2006).
[10] F. Zhou, K. Kang, T. Maxisch, G. Ceder, and D. Morgan, Solid State Commun. **132**, 181 (2004).
[11] R. Dominko, M. Gaberscek, J. Drofenik, M. Bele, and J. Jamnik, Electrochem. Acta **48**, 3709 (2003).
[12] S. L. Bewlay, K. Konstantinov, G. X. Wang, S. X. Dou, and H. K. Liu, Mater. Lett. **58**, 1788 (2004).
[13] S. Y. Chung, J. T. Bloking, and Y. M. Chiang, Nat. Mater. **1**, 123 (2002).
[14] S. Q. Shi, L. J. Liu, C. Y. Ouyang, D. S. Wang, Z. X. Wang, L. Q. Chen, and X. J. Huang, Phys. Rev. B **68**, 195108 (2003).
[15] P. S. Herle, B. Ellis, N. Coombs, and L. F. Nazar, Nat. Mater. **3**, 147 (2004).
[16] R. P. Santoro and R. E. Newnham, Acta Crystallogr. **22,** 344 (1967).
[17] G. Rousse, J. Rodriguez-Carvajal, S. Patoux, and C. Masquelier, Chem. Mater. **15**, 4082 (2003).
[18] D. Vaknin, J. L. Zarestky, L. L. Miller, J.-P. Rivera, and H. Schmid, Phys. Rev. B **65**, 224414 (2002).
[19] G. Liang, K. Park, J. Li, R. E. Benson, D. Vaknin, J. T. Markert, and M. C. Croft, Phys. Rev. B **77**, 064414 (2006).
[20] J. Li, V. O. Garlea, J. L. Zarestky, and D. Vaknin, Phys. Rev. B **73**, 024410 (2006).
[21] T. B. S. Jensen, N. B. Christensen, M. Kenzelmann, H. M. Rønnow, C. Niedermayer, N. H. Andersen, K. Lefmann, M. Jiménez-Ruiz, F. Demmel, J. Li, J. L. Zarestky, and D. Vaknin, Phys. Rev. B **79**, 092413 (2009).
[22] R. P. Santoro, D. J. Segal, and R. E. Newman, J. Phys. Chem. Solids **27**, 1192 (1966).
[23] S. Q. Shi, C. Y. Ouyang, Z. H. Xiong, L. J. Liu, Z. X. Wang, H. Li, D. S. Wang, L. Q. Chen, and X. J. Huang, Phys. Rev. B **71**, 144404 (2007).
[24] P. Tang and N. A. W. Holzwarth, Phys. Rev. B **68** 165107 (2003).
[25] K. Yamauchi and S. Picozzi, Phys. Rev. B **81**, 024110 (2010).
[26] P. E. Blöhl, Phys. Rev. B **50**, 17953 (1994).
[27] G. Kresse and J. Furthmüller, Phys. Rev. B **54**, 11169 (1996).
[28] J. P. Perdew, K. Burke, and M. Ernzerhof, Phys. Rev. Lett. **77**, 3865 (1996).
[29] A. I. Liechtenstein, V. I. Anisimov, and J. Zaanen, Phys. Rev. B **52**, R5467 (1995).
[30] V. I. Anisimov, I. V. Solovyev, M. A. Korotin, M. T. Czyzyk, and G. A. Sawatzky, Phys. Rev. B **48**, 16929 (1993).
[31] V. I. Anisimov, J. Zaanen, and O. K. Andersen, Phys. Rev. B **44**, 943 (1991).
[32] H. J. Monkhorst and J. D. Pack, Phys. Rev. B **13**, 5188 (1976).
[33] M. Methfessel and A. T. Paxton, Phys. Rev. B **40**, 3616 (1989).
[34] V. A. Streltsov, E. L. Belokoneva, V. G. Tsirelson, N. K. Hansen, Acta Crystallogr., Sect. B: Struct. Sci. **49**, 147 (1993).
[35] Ch. Delacourt, Ph. Poizot, J.-M. Tarascon, Ch. Masquelier, Nat. Mater. **4**, 254 (2005).
[36] Ch. Delacourt, J. Rodriguez-Carvajal, B. Schmitt, J.-M. Tarascon, and Ch. Masquelier, Solid State Sci. **7**, 1506 (2005).
[37] G. Chen, X. Song, and T. J. Richardson, Electrochem. Solid-State Lett. **9**, A295 (2006).
[38] C. Y. Ouyang, S. Q. Shi, Z. X. Wang, X. J. Huang, and L. Q. Chen, Phys. Rev. B **69**, 104303 (2004).
[39] Y. N. Xu, S. Y. Chung, J. T. Bloking, Y. M. Chiang, and W. Y. Ching, Electrochem. Solid-State Lett. **7**, A131 (2004).
[40] A. Hunt, W. -Y. Ching, Y. -M. Chiang, and A. Moewes, Phys. Rev. B **73**, 205120 (2006).
[41] D. Wang, H. Li, S. Shi, X. Huang, L. Chen, Electrochim. Acta **50**, 2955 (2005).
[42] T. Nakamura, Y. Miwa, M. Tabuchi, and Y. Yamada, J. Electrochem. Soc. **153,** A1108 (2006).